



Article

Rapid Lactic Acid Content Detection in Secondary Fermentation of Maize Silage Using Colorimetric Sensor Array Combined with Hyperspectral Imaging

Xiaoyu Xue ^{1,2}, Haiqing Tian ^{1,2,*}, Kai Zhao ^{1,2}, Yang Yu ^{1,2} , Ziqing Xiao ^{1,2}, Chunxiang Zhuo ^{1,2}  and Jianying Sun ^{1,2}

¹ College of Mechanical and Electrical Engineering, Inner Mongolia Agricultural University, Hohhot 010010, China; xiaoyuxue@emails.imau.edu.cn (X.X.); lat41n_zk@emails.imau.edu.cn (K.Z.); yuyangyq1997@emails.imau.edu.cn (Y.Y.); xiaozqnd@emails.imau.edu.cn (Z.X.); zcx@emails.imau.edu.cn (C.Z.); sjy031026@163.com (J.S.)

² Inner Mongolia Engineering Research Center of Intelligent Equipment for the Entire Process of Forage and Feed Production, Hohhot 010018, China

* Correspondence: hqtian@126.com

Abstract: Lactic acid content is a crucial indicator for evaluating maize silage quality, and its accurate detection is essential for ensuring product quality. In this study, a quantitative prediction model for the change of lactic acid content during the secondary fermentation of maize silage was constructed based on a colorimetric sensor array (CSA) combined with hyperspectral imaging. Volatile odor information from maize silage samples with different days of aerobic exposure was obtained using CSA and recorded by a hyperspectral imaging (HSI) system. Subsequently, the acquired spectral data were subjected to preprocessing through five distinct methods before being modeled using partial least squares regression (PLSR). The coronavirus herd immunity optimizer (CHIO) algorithm was introduced to screen three color-sensitive dyes that are more sensitive to changes in lactic acid content of maize silage. To minimize model redundancy, three algorithms, such as competitive adaptive reweighted sampling (CARS), were used to extract the characteristic wavelengths of the three dyes, and the combination of the characteristic wavelengths obtained by each algorithm was used as an input variable to build an analytical model for quantitative prediction of the lactic acid content by support vector regression (SVR). Moreover, two optimization algorithms, namely grid search (GS) and crested porcupine optimizer (CPO), were compared to determine their effectiveness in optimizing the parameters of the SVR model. The results showed that the prediction accuracy of the model can be significantly improved by choosing appropriate pretreatment methods for different color-sensitive dyes. The CARS-CPO-SVR model had better prediction, with a prediction set determination coefficient (R_p^2), root mean square error of prediction ($RMSEP$), and a ratio of performance to deviation (RPD) of 0.9617, 2.0057, and 5.1997, respectively. These comprehensive findings confirm the viability of integrating CSA with hyperspectral imaging to accurately quantify the lactic acid content in silage, providing a scientific and novel method for maize silage quality testing.

Keywords: lactic acid content; maize silage; colorimetric sensor array; hyperspectral images; non-destructive detection



Citation: Xue, X.; Tian, H.; Zhao, K.; Yu, Y.; Xiao, Z.; Zhuo, C.; Sun, J. Rapid Lactic Acid Content Detection in Secondary Fermentation of Maize Silage Using Colorimetric Sensor Array Combined with Hyperspectral Imaging. *Agriculture* **2024**, *14*, 1653. <https://doi.org/10.3390/agriculture14091653>

Academic Editor: Anna Andolfi

Received: 16 August 2024

Revised: 10 September 2024

Accepted: 20 September 2024

Published: 22 September 2024



Copyright: © 2024 by the authors. Licensee MDPI, Basel, Switzerland. This article is an open access article distributed under the terms and conditions of the Creative Commons Attribution (CC BY) license (<https://creativecommons.org/licenses/by/4.0/>).

1. Introduction

Along with the increasing demand for animal meat, eggs and milk in many developing countries, feedstuff deficiency has become an important factor limiting the development of livestock farming in most countries [1,2]. Silage represents a vital method of feed preservation in which green fodder undergoes fermentation to maintain a consistent nutrient supply for livestock during periods of feed scarcity [3,4]. Maize silage, a nutrient-dense

livestock feed, provides superior yields and energy densities at a reduced cost relative to alternative feed sources [5]. The fermentation of maize silage is governed by a diverse array of microorganisms and is influenced by several factors, including anaerobic conditions within the silo, the concentration of water-soluble compounds (WSC), and the content of dry matter. Silage relies heavily on lactic acid bacteria to convert soluble carbohydrates into lactic acid, which can reduce the pH to a level that inhibits undesirable fermentation that produces butyric acid and degrades amino acids, allowing for forage preservation and improved palatability [6]. Lactic acid plays a key role in maize silage production and can improve silage quality and stability through the mechanism of acidification. In general, a sign of good silage is a high lactic acid concentration. Consequently, the lactic acid content is a critical indicator for evaluating the fermentation quality of maize silage. However, inadequate sealing and oxygen infiltration during collection can compromise the anaerobic fermentation environment of silage, allowing aerobic microorganisms to proliferate extensively [7,8]. This triggers secondary fermentation, reduces the lactic acid content, and ultimately results in the degradation and spoilage of the maize silage. Deterioration of silage not only results in nutrient loss, which impairs nutrient absorption and diminishes animal production performance, but also may pose a health risk to consumers [9]. Therefore, precise monitoring of lactic acid content fluctuations in silage maize during secondary fermentation can elucidate the extent of aerobic deterioration.

Predominant techniques for measuring lactic acid content in maize silage encompass high performance liquid chromatography (HPLC), enzymatic methods, and gas chromatography (GC) [10]. Chromatography enables highly sensitive quantitative analysis of a diverse array of organic acids; however, the sample pre-treatment process is intricate, the detection period is extended, and it demands significant technical expertise from the personnel conducting the measurements. Enzymatic methods offers high specificity for lactic acid; however, the enzymes employed are costly, possess limited shelf lives, and require precise handling to prevent enzymatic degradation during analysis. Although the aforementioned methods are precise and yield minimal errors, they are destructive to the samples during actual measurements. Consequently, there is an imperative need to develop a novel method for the rapid, precise, and non-destructive assessment of lactic acid content in maize silage.

Colorimetric sensor array (CSA) is a new non-destructive detection technique for identifying complex volatile compounds based on the human olfactory principle [11,12]. It can form a special composite response to odors through the cross-reaction between the sensor and the volatile gases of the object to be measured, ultimately realizing the differentiation and detection of a wide range of chemical substances [13]. CSA is currently utilized extensively in the realms of agricultural safety and food quality analysis [14–16], particularly for assessing the freshness of meat and beer [17,18], as well as determining the storage durations of rice and wheat seeds [19,20]. Liu et al. [21] employed colorimetric sensor technology for the nondestructive detection of AFB1 in maize. They optimized the SVR model parameters using the particle swarm optimization (PSO) algorithm, which showed excellent predictive performance with R_p^2 of 0.99 and $RMSEP$ of 2.8. Jiang et al. [22] developed a quantitative model for assessing the content of tea polyphenols in green tea based on an olfactory visualization technique by combining the ant colony optimization (ACO) algorithm with an extreme learning machine (ELM), which achieved an R_p^2 of 0.8035. Zhao et al. [23] used an olfactory visualization technique combined with an SVR model and optimized the SVR model parameters with the Dungeness bug optimization (DBO) algorithm to obtain a corn moisture content prediction model with higher accuracy. However, the change information obtained based on the colorimetric sensor array technique is mainly characterized by extracting the RGB difference images before and after the reaction by a CCD camera, and the color change of each color-sensitive material is only characterized by the R, G, and B components. This lesser amount of information may not provide sufficient features to characterize the reaction between dyes and volatile

compounds. Therefore, it is necessary to introduce a new information collection technique to build quantitative predictive models from a more multidimensional data level.

The combination of spectroscopic and colorimetric sensing techniques can provide important information for the rapid detection of complex analytes [24,25]. An et al. [26] used CSA combined with hyperspectral imaging to collect odor information of different fermentation times of black tea and used an SVR model to score the aroma quality, and its prediction set discrimination rate reached 94.29%. Wang et al. [27] used a CSA based on a pH indicator combined with hyperspectral imaging to intelligently assess the degree of wilting, and the best discriminative results were obtained based on a least squares support vector machine (LSSVM) model. Li et al. [28] developed a colorimetric sensor array-coupled hyperspectral imaging system for rapid quantitative prediction of key volatile organic compounds (VOCs) in black tea. A LSSVM model was built with the characteristic wavelengths screened by CARS as inputs, and the correlation coefficients of linalool, phenylglyoxal, hexanal, methyl salicylate and geraniol were 0.89, 0.95, 0.88, 0.80 and 0.78, respectively. However, most current research typically employs a single algorithm to preprocess spectral data across multiple dyes, with limited investigations into the optimal preprocessing methods tailored for different dyes. Therefore, it is necessary to find the best pretreatment method for each dye.

In fact, differences in lactic acid content of maize silage during secondary fermentation can directly influence changes in their internal components, including fatty acids and proteins. Modifications in the feed's ingredients exert a direct influence on both the composition and content of volatile substances emanating from it. Therefore, it is theoretically feasible to utilize CSA in combination with HSI technology to achieve quantitative analysis of feed lactic acid content. To date, there are few reports in the literature on the use of CSA combined with HSI to quantitatively predict the lactic acid content of maize silage. Based on the above analysis, the main work of this study was as follows: (1) Preparation of 5×4 sensor array using 17 color sensitive dyes. (2) Using an HSI system to obtain the spectral data of the color dyes after the reaction, preprocessing the data using Savitzky–Golay (SG) smoothing and five other algorithms, and establishing a PLSR model to identify the optimal preprocessing algorithm for each dye. (3) The CHIO algorithm was introduced to screen three dyes sensitive to lactate values. (4) Three algorithms, including CARS, were utilized to screen the variables of each dye's spectral data and construct a SVR model to quantitatively detect the lactic acid content of maize silage. In this process, the focus was on the optimization capabilities of the grid search (GS) and crested porcupine optimizer (CPO) algorithms for SVR model parameters.

2. Materials and Methods

2.1. Sample Preparation

The maize silage forage samples used in this study were purchased in three batches, each weighing 50 kg, for a total of 150 kg. The silage samples purchased in the first batch were preserved in a cellar and were procured from Donghuaying Village, Tuzuo Banner, Hohhot City, Inner Mongolia, China (111°58' E, 40°58' N), variety Kehe 696. The maize silage purchased for the last two batches was stored using the film-wrapping method and was procured from Taihe County, Fuyang City, Anhui Province, China (115°80' E, 33°38' N), from the varieties Jingza442 and Hong sai4. The storage temperature, storage time, and kernel composition of the maize silage samples remained consistent throughout the experiment.

To simulate the secondary fermentation process of maize silage, the collected samples were subjected to continuous aerobic exposure. Undelayed maize silage was placed in polyethylene boxes at 3 kg (± 100 g) per box, with a total of 16 boxes prepared for each trial. To prevent evaporation of moisture and at the same time to ensure air circulation, the polyethylene box was covered with aluminum foil with evenly distributed small holes. Sixteen boxes of maize silage were then divided into 0D–7D aerobic exposure groups in groups of two boxes. For each day's sampling, the maize silage in the polyethylene

boxes was evenly divided into three sections, and three samples were taken from each box, culminating in a comprehensive collection of 144 samples prepared for analysis. Sample preparation and data analysis are shown in Figure 1.

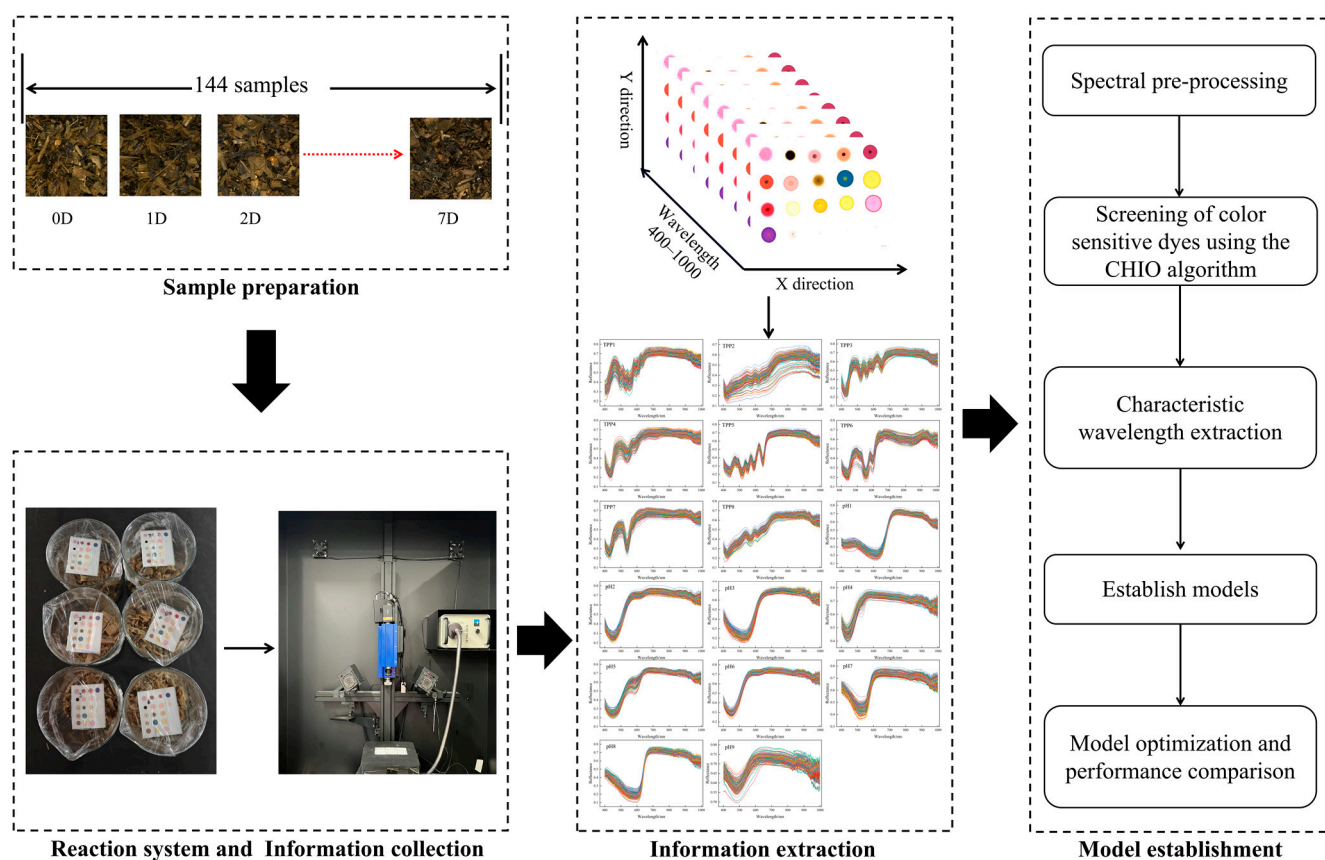


Figure 1. Experiment and data analysis flowchart.

2.2. Determination of Lactic Acid Content of Maize Silage

In this study, high performance liquid chromatography (HPLC) was used to determine the lactic acid content of the maize silage samples with reference to DB15/T 1458-2018 [29]. The equipment used was a high-performance liquid chromatograph (LC-20AT, Shimadzu Corporation, Kyoto, Japan).

2.3. Preparation of Colorimetric Sensor Array

Preparation of CSA using appropriate color-sensitive dyes can improve the detection accuracy of the technique. Therefore, color-sensitive dyes for the preparation of CSA need to meet the following requirements: (1) Have a chemical group capable of reacting with the substance to be measured; and (2) The reaction with the substance to be measured is accompanied by a distinct color change. Based on the halo effect and response observed in preliminary experiments, eight TPPs and nine pH indicators were chosen, totaling 17 color-sensitive dyes for the CSA. Essential details regarding the color-sensitive dyes utilized for the sensor array preparation are presented in Table 1.

The detailed procedures for CSA preparation are as follows: Initially, 10 mg each of TPP and pH indicator were dissolved in 5 mL of dichloromethane and anhydrous ethanol, respectively, achieving a mass concentration of 2 mg/mL for each solution. The prepared solution was hermetically sealed within a reagent bottle, placed in an ultrasonic shaker, and shaken for 20 min to ensure complete dissolution of both the porphyrin and the pH indicator. In order to minimize the influence of ambient humidity on the sensor accuracy, a C2 reverse silica gel plate (Merck KGaA, Frankfurter, Germany) with good hydrophobicity was chosen as the sensor carrier, and its tiny pore size can also help to adsorb gas molecules

to accelerate the detection speed. A 5×4 sensor array was assembled by extracting $1 \mu\text{L}$ of solution using a 100×0.3 mm capillary and applying it to spot-stain 17 color-sensitive dyes onto a 4×3 cm C2 reverse silica gel plate. Ultimately, the fabricated sensor array was placed in a fume hood for 30 min to stabilize, then preserved in a hermetically sealed bag at a low temperature.

Table 1. Information on color-sensitive dyes in CSA.

Number	Name
1	2,3,7,8,12,13,17,18-Octaethyl-21h,23h-porphine
2	5,10,15,20-Tetrakis (4-carboxyphenyl)-porphyrin-Fe-(iii)-chloride
3	5,10,15,20-Tetrakis (4-methoxyphenyl)-21,22-dihydroporphyrin
4	5,10,15,20-Tetrakis (4-methoxyphenyl)-21h,23h-porphyrine-cobalt(ii)
5	5,10,15,20-Tetraphenyl-21h,23h-porphyrin
6	5,10,15,20-Tetraphenyl-21,22-dihydroporphyrin zinc
7	5,10,15,20-Tetraphenyl-21h,23h-porphine copper(II)
8	5,10,15,20-Tetraphenyl-21h,23h-porphine iron(iii) chloride
9	Bromocresol Green
10	Bromothymol Blue
11	Neutral Red
12	Cresol Red
13	Bromocresol Purple
14	Thymol Blue
15	Methyl Red
16	Bromophenol Blue
17	Congo Red

2.4. Hyperspectral Image Acquisition and Preprocessing of Colorimetric Sensor Array

Each portion of the maize silage forage was mixed well and reduced using the tetrad method until the sample was reduced to 50.0 g (accurate to 0.1 g). The prepared 50 g maize silage samples were positioned in a glass beaker with a 60 mm diameter. As shown in Figure 1, the sensor silica gel plate was affixed to the cling film using double-sided adhesive, and the cling film was sealed over the beaker's opening to ensure full exposure of the sensors to the volatile gas environment. The reaction proceeded at room temperature for 15 min.

In this study, the spectral data of the color-sensitive dye sites were obtained using the HSI system, as shown in Figure 1. The system mainly consists of a hyperspectral image spectrometer (ImSpector Model V10E, Spectral Imaging Ltd., Oulu, Finland), a CCD camera (Model IGV-B1620, Imperx, Boca Raton, FL, USA), six halogen lamps (for three 50 W lamps per group) (DECOSTAR® 51 STANDARD, OSRAM Ltd., Munich, Germany), and a mobile control platform (IRCP0076-1COM, ISUZU Optics Co., Ltd., Taiwan, China). The hyperspectral imaging (HSI) system was started and warmed up for 30 min prior to data acquisition. Afterward, the light source and lens were adjusted so that the capture position was in the center of the experimental platform and the sensor could be captured in its entirety. The system exposure time is 1.2 ms when acquiring hyperspectral images. In order to eliminate the effects of light inhomogeneity and dark current noise, the raw spectral image was corrected with the following equation:

$$R = \frac{I_S - I_D}{I_W - I_D} \quad (1)$$

where R is the black-and-white corrected sample image; I_S is the original image of the sample; I_D is the dark reference image obtained by overlaying the lens; and I_W is the reference image obtained by a standard calibration whiteboard. After calibration, the average spectra of the visible hyperspectral images of the CSA were extracted using ENVI 5.6 (ITT Visual Information Solutions, Boulder, CO, USA), and each dye region in the image

was selected as a region of interest (ROI). The average spectral information of all pixel points in the ROI was used as the raw spectral information.

2.5. Spectral Data Preprocessing

In the process of hyperspectral image acquisition, the spectral signal will be interfered with by stray light, noise, baseline drift and other factors due to the performance of the hyperspectral camera and the measurement environment. In order to eliminate the interference and establish a stable and reliable model, it is necessary to preprocess the spectral data [30]. In this study, five methods, Savitzky–Golay (SG) smoothing, the standard normal variate (SNV) method, multiplicative scatter correction (MSC), first-order derivation method (FD), and second-order derivation method (SD), were utilized to preprocess the spectral data, and PLSR was used for modeling. The R^2 was used as an evaluation index for the preprocessing screening.

2.6. Data Analysis Methods

2.6.1. Coronavirus Herd Immunity Optimizer (CHIO)

CHIO is an optimization algorithm based on herd immunity strategies to simulate the process of the new coronavirus transmission and immune formation [31]. The algorithm controls virus transmission between individuals through basic reproduction rate (BRr) and MaxAge of infection and updates the genetic values of individuals based on social distancing strategies to search for a globally optimal solution in the solution space. CHIO iteratively updates the state of an individual by exploiting susceptible, infected, and immune interactions of susceptible, infected, and immune individuals and stops when the maximum number of iterations is reached in order to solve the global optimization problem efficiently.

In this study, SVR was embedded as a regressor in the CHIO algorithm with the aim of identifying the characteristic wavelengths of color-sensitive dyes that are closely related to the lactic acid content of maize silage. This study intended to independently execute the algorithm 50 times, and the frequency of the selected features of each dye in each run was recorded to screen dyes sensitive to lactic acid content. When the CHIO algorithm was applied, the bacterial population size was 50, the BRr parameter was set to 0.15, the MaxAge parameter was set to 10, and the maximum number of iterations of the algorithm was 100.

2.6.2. Crested Porcupine Optimizer (CPO)

CPO is a novel meta-heuristic algorithm inspired by the defensive behavior of porcupines [32]. In this study, the CPO algorithm was used to optimize the parameters of the support vector regression (SVR) model to improve the accuracy of the prediction of lactic acid content in maize silage based on CSA combined with HSI technique. The algorithm simulates the four main defense strategies of the porcupine—sight, sound, smell, and physical attack—corresponding to the different stages of the optimization process. Visual and acoustic strategies are used for exploration, helping to investigate different areas of the search space, while odor and physical attack strategies are used for exploitation, fine-tuned for specific areas. The algorithm proposes a new strategy called the cyclic population reduction technique, which mimics the selective activation of defense mechanisms by porcupines when threatened in order to maintain population diversity and accelerate the convergence process. The mathematical model of the strategy is as follows:

$$N = N_{\min} + (N' - N_{\min}) \times \left(1 - \left(\frac{t\% \frac{T_{\max}}{T}}{\frac{T_{\max}}{T}} \right) \right) \quad (2)$$

where T is the variable that determines the number of cycles, t is the current function evaluation, T_{\max} is the maximum number of function evaluations, N' denotes the number of individuals, and N_{\min} is the minimum number of individuals in the newly generated

population. The parameters of the optimization algorithm were set as follows: the maximum number of iterations was 50, the lower limit was [0.1, 0.1], and the upper limit was [50, 50]. The specific steps of model optimization were as follows:

Step 1: Initialize the number of populations and iterations in the CPO and the parameters c and g of the SVR model for predicting maize silage lactate content.

Step 2: An initial population was generated, with the position of each porcupine corresponding to a randomly generated set of SVR parameters.

Step 3: Using the mean square error of the prediction set as the objective function, the performance of each porcupine was evaluated, and the location of the porcupine with the smallest MSE value was selected as the current optimal solution.

Step 4: The other “porcupines” update their positions according to the position of the optimal solution, a process that mimics the porcupine’s defense strategy. The population size was dynamically adjusted through a cyclic population reduction technique to balance exploration and exploitation. During the exploration phase, the visual and acoustic defense strategies of the porcupine were simulated by adjusting the values of c and g to expand the search area and increase the diversity of the solution space. During the development phase, the porcupine’s scent and physical attack defense strategies were simulated, the hyperparameters c and g were finely tuned to be close to the current best solution for further optimization, and the parameters were aggressively adjusted to ensure that the globally optimal solution was found.

Step 5: Steps 3 and 4 were performed consecutively until the predetermined maximum number of iterations was reached.

2.6.3. Feature Variable Screening

Spectral data collected by a spectrometer usually contains hundreds or even thousands of data points, and this large-scale data volume can significantly increase the difficulty of computation and the complexity of the model. To cope with this problem, data compression and feature extraction methods are usually used to extract effective information. These methods not only reduce the amount of computation but also improve the accuracy and robustness of the model by simplifying the model structure. Feature extraction techniques can effectively filter out the most representative wavelengths, thus retaining the most valuable information for model prediction while removing redundancy and noise. In this study, several methods were used to extract the characteristic wavelengths: the competitive adaptive reweighted sampling (CARS) algorithm, the iterative retained information variable (IRIV) algorithm, and the variable combination population analysis (VCPA) algorithm [33]. Each of these methods has its own characteristics, and the most representative characteristic wavelengths were screened out by different strategies, which effectively reduced the data redundancy and thus improved the prediction accuracy and computational efficiency of the model.

When using the CARS algorithm, the number of Monte Carlo samples was set to 50 and the number of cross-validations was 5. When using the IRIV algorithm, the number of cross-validations was set to 5 and the maximum number of principal components was 10. When using the VCPA algorithm, a 5-fold cross-validation method was used with the number of BMS runs set to 1000 and the number of EDF runs set to 50.

2.6.4. Support Vector Regression (SVR)

SVR is a variant of support vector machines (SVM) specifically designed for function regression fitting. In contrast to traditional regression techniques, SVR is formulated using a nonlinear approach, enabling it to adeptly manage nonlinear regression problems. SVR maps the data into a high-dimensional data feature space using a nonlinear mapping, resulting in a good linear regression of the independent variable to the dependent variable in the high-dimensional data feature space, where it is fitted and then returned to the original space [34].

Several studies have shown that the performance of SVR depends heavily on the chosen form of the kernel function, the penalty factor (C), and the kernel parameters (g) [35]. Radial basis functions tend to give better predictions without the guidance of prior knowledge. Therefore, we chose the radial basis function as the kernel function. To identify the appropriate parameters, this study used grid search (GS) to find the optimal combination of (c, g) through 5-fold cross-validation. The GS method took the value range of $[2^{-10}, 2^{10}]$ and the grid search step was $2^{0.5}$.

2.6.5. Partial Least Squares Regression (PLSR)

The PLSR method is one of the most effective linear multivariate calibration algorithms. It can solve the problem of multicollinearity due to many variables. The PLSR model projects high-dimensional data onto several independent latent variables (LVs) that contain most of the information in the original data. In practice, the impact of models containing different numbers of LVs on the predictive performance is usually assessed by cross-validation methods to determine the number of LVs [36]. The number of LVs for each PLSR model takes the value range of [1, 35].

K-fold cross-validation is extensively used to find the best machine learning algorithm with optimal parameters [37]. The method involves dividing all samples in the training set into K folds, using K-1 folds for training and the remaining fold for validation, and repeating this process K times. In this study, a 5-fold cross-validation method was used and the constructed optimal model was externally validated using samples from the prediction set. In the PLSR model and the SVR model, the averages of the RMSE and MSE values of the K validations were taken as the results, respectively. Smaller RMSE and MSE values indicate better generalization capability of the model. Finally, the parameter with the smallest RMSE and MSE values was selected as the optimal parameter of the model.

2.6.6. Model Evaluation

To accurately evaluate the precision and robustness of the developed model, this study used the Kennard–Stone (K-S) algorithm to divide the collected 144 samples into training and prediction sets on a 4:1 basis. A prediction model for the lactic acid content of maize silage was constructed by means of support vector machine regression using the reflectance of the three screened dyes as the main inputs, and the validity of the model was assessed by a combination of the coefficient of determination (R^2), the root mean square error of the training set ($RMSEC$), the root mean square error of the prediction set ($RMSEP$), and the ratio of the performance to deviation (RPD) values. Among them, the closer the R^2 value is to 1, the higher the stability and fit of the model is; and the closer the $RMSEC$ and $RMSEP$ values are to 0, the stronger the predictive ability of the model is. The RPD value is obtained by calculating the ratio of the standard deviation of the samples to the root mean square error, and if the $RPD < 1.5$, the model cannot implement the prediction of the samples. When $1.5 \leq RPD < 2.0$, the model can carry out a rough assessment of the samples, and when $2.0 \leq RPD < 3.0$, the model can carry out an excellent prediction of the samples. When $RPD \geq 3$, the model can carry out a very good prediction of the samples [38].

3. Results and Discussion

3.1. Changes in Lactic Acid Content during Secondary Fermentation

Figure 2 elucidates the relationship between lactic acid content and aerobic exposure time during the secondary fermentation of maize silage. The lactic acid content tended to decrease with increasing aerobic exposure time. During the secondary fermentation of silage, the lactic acid content showed a clear phase change. The lactic acid content was higher on day 0, about 40 mg/g, before the silage was exposed to air. This phenomenon indicates that the silage was in a good state of fermentation before it was exposed to air, and the lactic acid bacteria showed high fermentation activity by producing large amounts of lactic acid during the fermentation process.

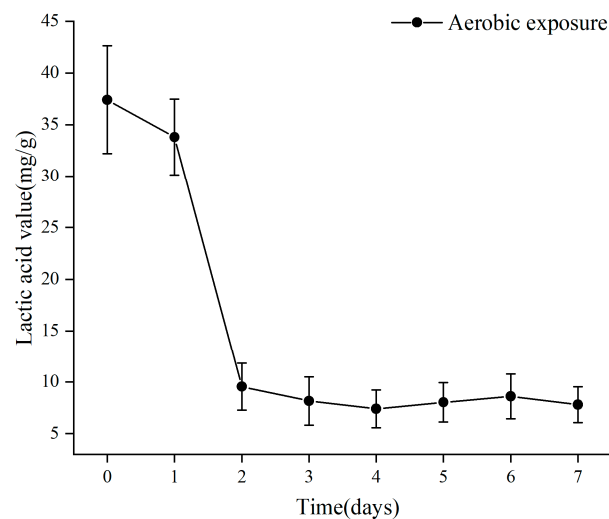


Figure 2. Changes in lactic acid content during secondary fermentation.

Between day 0 and day 2 after the start of the exposure, the sensory properties of the maize silage began to deteriorate and the lactic acid content dropped dramatically, from about 40 mg/g to less than 10 mg/g. The sharp decrease in lactic acid content during this period may be due to the exposure of silage to air, where the entry of oxygen promotes the rapid multiplication and metabolic activity of aerobic microorganisms such as yeasts and molds. These aerobic microorganisms utilize lactic acid as a source of energy and produce carbon dioxide and water, leading to rapid depletion of lactic acid and a rise in pH. The dramatic changes in this phase reflect the peak of microbial activity at the beginning of the exposure and the fastest rate of lactic acid degradation. From day 2 onwards, the lactic acid content enters a phase of relative stabilization, remaining between 5 and 10 mg/g. At this stage, the degradation of lactic acid slowed down significantly, probably due to the fact that after the initial large amount of lactic acid was consumed, the remaining lactic acid was no longer sufficient to support large-scale aerobic microbial reproduction. Meanwhile, microbial activities gradually reached an equilibrium state. During this period, residual lactic acid bacteria continue to produce lactic acid under localized anaerobic conditions, but at a reduced rate. The maize silage is sticky and clumpy and emits a foul odor.

It has been shown that changes in the lactic acid content of silage during aerobic exposure are mainly influenced by microbial activity and environmental conditions. During the initial period of exposure, the lactic acid content decreased dramatically due to the active metabolism of aerobic microorganisms. Subsequently, the lactic acid content stabilized as the microbial activity gradually reached a state of equilibrium. These results are important for understanding the deterioration mechanisms of silage during exposure. In practice, samples are taken during the pick-up process to quickly determine the lactic acid content of the maize silage, which enables the managers to keep abreast of the state of fermentation of the maize silage in the silo. If abnormal lactic acid levels are detected in a sample it is possible to intervene in time to minimize losses. Conventional assays often require expensive consumables (e.g., solvents, columns) and the assay setup for each sample is time-consuming and destructive. This study combined CSA and HSI techniques to analyze multiple samples quickly and non-destructively, without the need for cumbersome sample pre-processing. In contrast to traditional methods, the method can be combined with analytical software that can be operated with simple training, thus reducing learning costs for practitioners.

3.2. Spectral Preprocessing Results

In this study, the 144 maize silage samples obtained for the experiment were divided into a training set and a prediction set in a ratio of 4:1.115 samples (training set) were used to calibrate the model and cross-validate, and the remaining 29 samples (prediction set)

were used to independently test the predictions. Table 2 shows the statistics of the lactic acid content of maize silage, where Max, Min and Mean denote the maximum, minimum and average values in the delineated dataset, respectively. As can be seen from Table 2, the target values of the two datasets are independent of each other and the differences between them are small and within acceptable limits.

Table 2. Statistical results of the measurement of the lactic acid content of the samples.

Sample Set	Sample Size	Max	Min	Mean	Standard Error
Total	144	47.5616	3.3529	15.0908	12.2613
Training set	115	47.5616	3.3529	15.7293	12.6423
Prediction set	29	44.0952	5.7385	12.5588	10.4291

Preprocessing of raw spectra is necessary to guarantee the validity of accurate chemometric models. In this paper, SG, MSC, SNV, FD and SD were chosen to preprocess the raw spectra of 17 dyes and PLSR was used for modeling, and the results are shown in Table 3.

Table 3. Predicted performance of 17 color-sensitive dyes preprocessing algorithms.

Number	LV	Raw Data		LV	SG		LV	SNV		LV	MSC		LV	FD		LV	SD	
		R _C ²	R _P ²		R _C ²	R _P ²		R _C ²	R _P ²		R _C ²	R _P ²		R _C ²	R _P ²		R _C ²	R _P ²
1	10	0.8896	0.7680	12	0.9272	0.7429	9	0.9225	0.7549	9	0.9241	0.7429	4	0.9031	0.7790	7	0.9926	0.7272
2	8	0.8622	0.4347	12	0.9343	0.7929	7	0.8629	0.7391	8	0.9155	0.7798	6	0.9868	0.5565	3	0.9417	0.4026
3	10	0.8896	0.5056	10	0.8968	0.8886	13	0.9769	0.6776	12	0.9672	0.6466	4	0.9217	0.6724	6	0.9873	0.5019
4	10	0.8736	0.7197	11	0.9173	0.7492	8	0.8428	0.6803	13	0.9724	0.7392	5	0.9439	0.6961	4	0.9775	0.4182
5	12	0.9728	0.6854	6	0.9034	0.7756	10	0.9574	0.8016	9	0.9367	0.7363	6	0.9701	0.7139	8	0.9972	0.4579
6	11	0.9019	0.4337	12	0.9178	0.5369	26	0.9999	0.7463	12	0.9399	0.7912	5	0.9318	0.6357	11	0.9994	0.5082
7	11	0.9007	0.3231	17	0.9462	0.8672	11	0.9462	0.4736	11	0.9294	0.5987	5	0.9379	0.6377	3	0.9374	0.6311
8	10	0.9226	0.4796	9	0.8885	0.7906	8	0.9171	0.5208	9	0.9332	0.6229	11	0.9997	0.7160	4	0.9824	0.7148
9	9	0.8523	0.6631	10	0.8895	0.8152	12	0.9668	0.6381	13	0.9778	0.5793	5	0.9575	0.8044	3	0.9447	0.5483
10	9	0.9155	0.7528	10	0.9235	0.7825	8	0.9212	0.8841	8	0.9198	0.8722	4	0.9610	0.8155	2	0.8903	0.6210
11	13	0.9792	0.7775	6	0.7844	0.6545	11	0.9775	0.7872	10	0.9667	0.7885	8	0.9943	0.6381	2	0.8936	0.4987
12	3	0.3419	0.4222	9	0.8530	0.7617	11	0.9672	0.7232	10	0.9540	0.7081	8	0.9972	0.3847	10	0.9993	0.5026
13	10	0.8290	0.6501	16	0.9456	0.7652	9	0.8481	0.5099	8	0.8021	0.5513	4	0.9393	0.3725	2	0.8942	0.3785
14	10	0.9419	0.6323	9	0.8931	0.8043	9	0.9523	0.7878	9	0.9529	0.7850	7	0.9951	0.8381	2	0.8786	0.6131
15	9	0.8950	0.5962	9	0.8991	0.7055	5	0.7730	0.7720	7	0.8789	0.7760	3	0.9322	0.7885	3	0.9461	0.7096
16	8	0.6966	0.4265	13	0.9372	1.453	11	0.9501	0.4432	8	0.8691	0.3430	6	0.9812	0.5055	8	0.9452	0.4432
17	7	0.6447	0.1306	14	0.9368	0.7210	8	0.8929	0.5283	8	0.8842	0.5917	4	1.0000	0.4702	4	0.9685	0.5348

As shown in Table 3, by analyzing the modeling results of each dye under different preprocessing methods, it can be found that the preprocessing methods have a significant effect on the modeling effect. The SG, MSC, and FD algorithms performed prominently for most of the dyes, while the SD algorithm showed a tendency of decreasing modeling accuracy for some of the dyes, which may be attributed to the fact that the algorithm amplifies the noise in the spectral data, resulting in a decrease in modeling accuracy. It was finally concluded that TPP#2, 3, 4, 7, 8 and pH#1, 4, 5, 9 had the best results after preprocessing with the SG algorithm, probably because after processing with SG, the spectral data were smoothed and the noise was reduced while the shape and trend of the signal was retained, thus improving the signal-to-noise ratio of the model and the prediction accuracy. TPP#6 and pH#3 showed the best results after MSC pretreatment, probably because after treatment with MSC, the light scattering effects caused by changes in particle size were corrected, the scattering variance in the spectra was reduced, the correlation with or physical properties was enhanced, and the stability and accuracy of the model were improved. TPP#5 and pH#2 showed the best results after SNV pretreatment, probably because the predictive performance of the model was improved after treatment with SNV by standardizing each spectrum, reducing scattering effects and baseline drift, and homogenizing the spectra between different samples. TPP#1, and pH#6, 7, 8 showed the best results after FD pretreatment, probably because treatment with FD highlighted the characteristic peaks of the spectra, reduced baseline drift and background noise, enhanced the spectral resolution, and improved the sensitivity and accuracy of the model. The results showed that choosing appropriate data preprocessing methods can effectively reduce the noise information in the original data and improve the model accuracy. Therefore, it is

preferred that the dye spectra that have been pre-treated as described above be used for subsequent modeling, and the dye pre-treated spectra are shown in Figure 3.

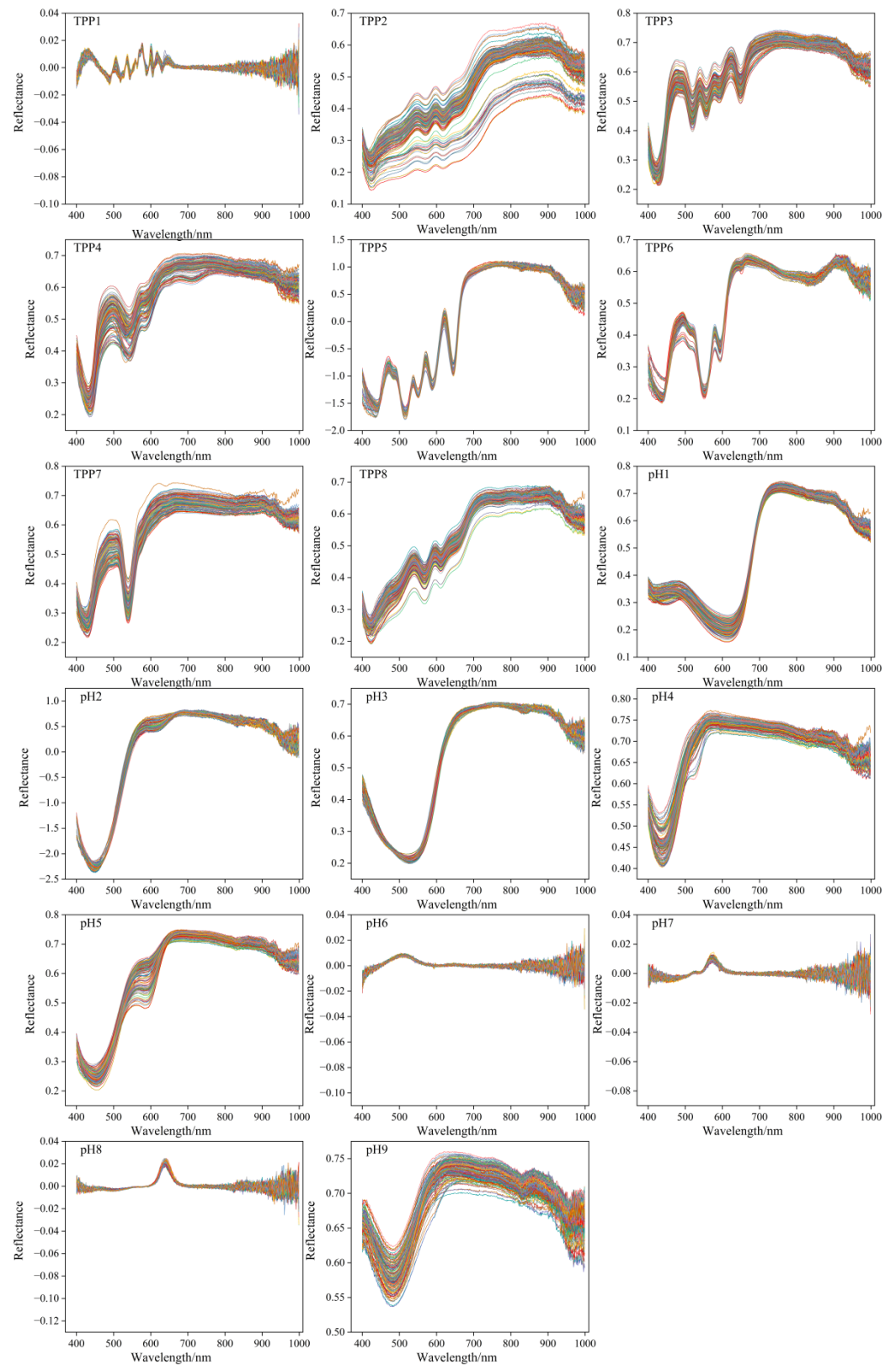


Figure 3. Spectral profiles of the optimally pretreated 17 dyes.

3.3. CHIO Dye Screening Results

The type and quantity of color-sensitive dyes for CSA is a key factor affecting non-destructive detection performance and fabrication cost, so it is particularly important to screen the sensor color-sensitive dyes. Figure 4a presents the images of the CSA, where 17 color-sensitive dyes were distributed on the C2 reverse silica gel plate with uniform colors. The CHIO algorithm was used to screen the color-sensitive dyes for CSA. Due to the randomness of the CHIO algorithm in the initialization of the parameters, the characteristic wavelengths selected by the CHIO algorithm will be somewhat different after each run. Therefore, in order to eliminate the negative impact of these random factors on the final results of the CHIO algorithm, this study proposed executing the algorithm independently 50 times and conducting a comprehensive analysis of the results after 50 runs. Figure 5 shows the statistics of the number of times each wavelength was selected for each dye after 50 runs using the CHIO algorithm. The CHIO algorithm selected the wavelengths corresponding to several dyes several times after 50 independent runs. For example, there were 55 wavelengths corresponding to pH#5 that had been selected more than 25 times. The 49 wavelengths corresponding to TPP#6 were selected more than 25 times, and the 46 wavelengths corresponding to TPP#8 were selected more than 25 times. It is worth noting that several dyes correspond to a small number of wavelength choices. For example, pH#8 corresponds to only 19 wavelengths selected more than 25 times. From a mathematical point of view, we can assume that dyes whose wavelengths have been selected multiple times are more sensitive to changes in volatile organic compounds produced during the secondary fermentation of maize silage. So TPP#6, 8 and pH#5 were used for subsequent studies. The distribution of the screened color-sensitive dyes on the C2 reverse silica gel plate is shown in Figure 4b.

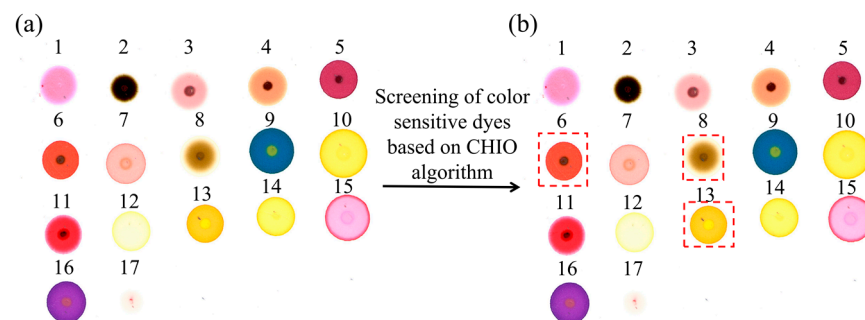


Figure 4. Screening of color sensitive dyes by CHIO algorithm. (a) Location distribution of sensor color-sensitive dyes; (b) Locations of the three color-sensitive dyes obtained by screening.

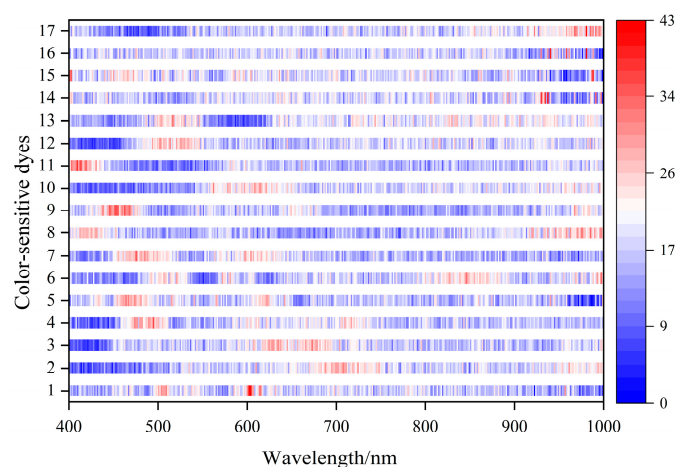


Figure 5. The total number of times each dye wavelength was selected after each run of the CHIO algorithm.

3.4. CSA Spectral Response Results

The primary factor affecting changes in the CSA is volatile gases, and changes in lactic acid content during secondary fermentation can have an effect on the volatile gas composition. Therefore, maize silage samples with different lactic acid contents produce different CSA spectral responses. As shown in Figure 6, the spectral curves of the color-sensitive dyes differed as the number of days of aerobic exposure increased. The spectral differences between TPP#8 and pH#5 were concentrated in the wavelength ranges of 485–550 nm and 540–600 nm, respectively, showing significant separation trends. The spectral differences of TPP#6 were mainly concentrated in the wavelength range of 400–450 nm, and its separation tendency was not as good as that of the first two dyes. This suggests that there is a valid correlation between lactic acid content and CSA in maize silage samples and that the associated pattern of change can be detected by the HSI technique.

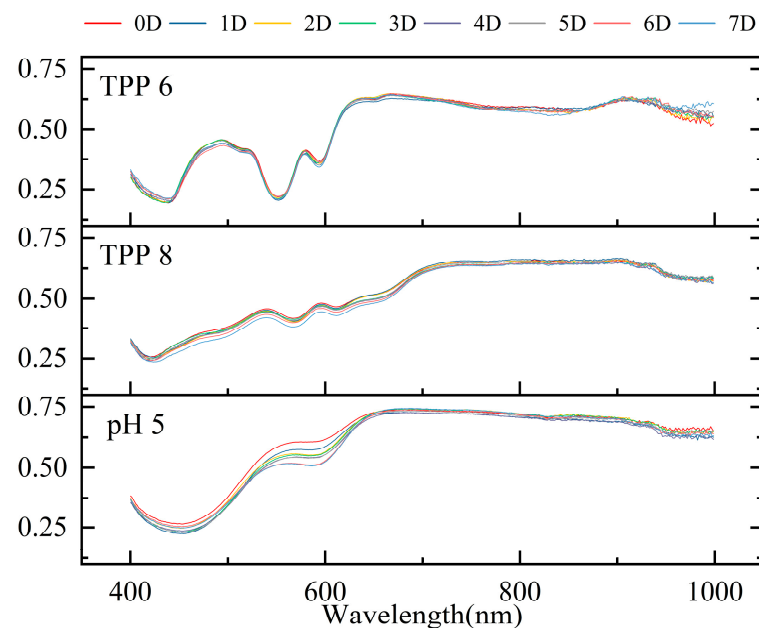


Figure 6. Spectral response of maize silage samples with different lactic acid contents.

3.5. Characteristic Wavelength Extraction Results

Based on the three color-sensitive dyes obtained from the screening of the CHIO algorithm, the pre-processed spectra were screened for variables using three methods: CARS, IRIV, and VCPA. The three preferred color-sensitive dye spectral curve characteristic variables selected by the different methods are shown in Figure 7. Vertical lines are used to indicate the position of the selected variable in the spectrum. The number of wavelength variables for each dye was 411. After CARS variable screening, the number of wavelength variables for TPP#6, 8 and pH#5 was reduced from 411 to 56, 46, and 94, respectively. Most of the wavelength variables in the original spectra that contributed little to the modeling were eliminated, and the screened wavelengths accounted for 13.6%, 11.2%, and 22.9% of the full spectrum, respectively. After IRIV variable screening, the number of wavelength variables for TPP#6, 8, and pH#5 was reduced from 411 to 73, 55, and 45, respectively, and the screened wavelengths accounted for 17.8%, 13.4%, and 10.9% of the full spectrum, respectively. After VCPA variable screening, the number of wavelength variables was reduced from 411 to 11, 10, and 11 for TPP#6, 8 and pH#5, respectively. The screened wavelengths accounted for 2.7%, 2.4%, and 2.7% of the full spectrum, respectively.

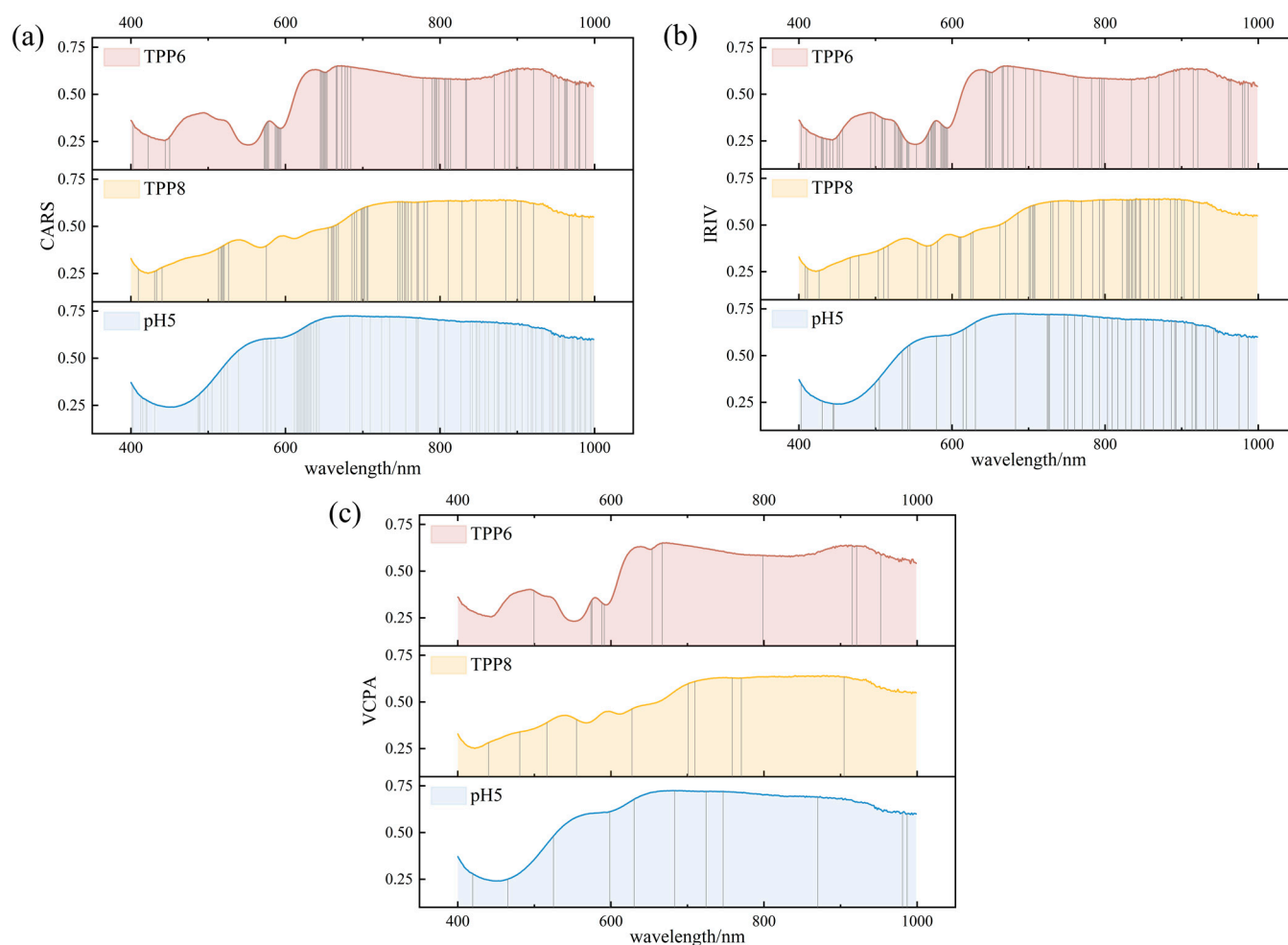


Figure 7. Variable selection results of the (a) CARS, (b) IRIV, and (c) VCPA screening methods.

As shown in Figure 7a, the CARS method exhibits high densities in feature extraction, especially in the wavelength ranges of 500–600 nm and 800–1000 nm, and most of these variables are distributed near the absorption peaks of the spectral curves. Compared to the CARS algorithm, the IRIV algorithm performs similarly in terms of consistency of feature extraction location and concentration of wavelength range, both being able to extract a large number of features in the 500–600 nm and 800–1000 nm wavelength ranges (shown in Figure 7b). As shown in Figure 7c, the VCPA method filters out the maximum number of variables compared to the CARS and IRIV methods.

3.6. Support Vector Regression Model Results under Different Optimization Algorithms

Based on the pre-processing of the three dyes obtained from the screening, the combinations of the characteristic wavelengths of the three dyes extracted by the CARS, IRIV and VCPA algorithms were used as model inputs to construct the GS-SVR model. The parameter optimization process and the regression between the predicted and measured values of the GS-SVR model for the three feature extraction algorithms are shown in Figure 8a,b,d,e,g,h. The accuracy of the GS-SVR model constructed by the three feature extraction algorithms was significantly improved compared to the GS-SVR model constructed using raw spectra. In the CARS-GS-SVR model, the model predicted best when the c value was 45.2548 and the g value was 0.0078, with coefficients of determination of 0.9873 and 0.9369 in the training and prediction sets, and $RMSEC$, $RMSEP$, and RPD of 1.4198, 2.5736, and 4.0523, respectively. The IRIV-GS-SVR model showed similar performance to the CARS-GS-SVR model, which is consistent with the results of the characteristic wavelength screening. The R_C^2 , R_P^2 , $RMSEC$, $RMSEP$, and RPD values were 0.9839, 0.9198, 1.5982, 2.9020, and 3.5938,

respectively, when the c value was 32 and the g value was 0.0110. When the value of c was 128 and g was 0.0156, the R_p^2 value of the VCPA-GS-SVR model was 0.8703, the $RMSEP$ value was 3.6900, and the RPD value was 2.8263. Under the conditions of GS optimization, the SVR model performance of the VCPA algorithm exhibited markedly inferior performance, evidenced by lower prediction set determination coefficients and heightened prediction errors, indicating that it falls short of the efficacy demonstrated by the CARS and IRIV algorithms in this optimization scenario.

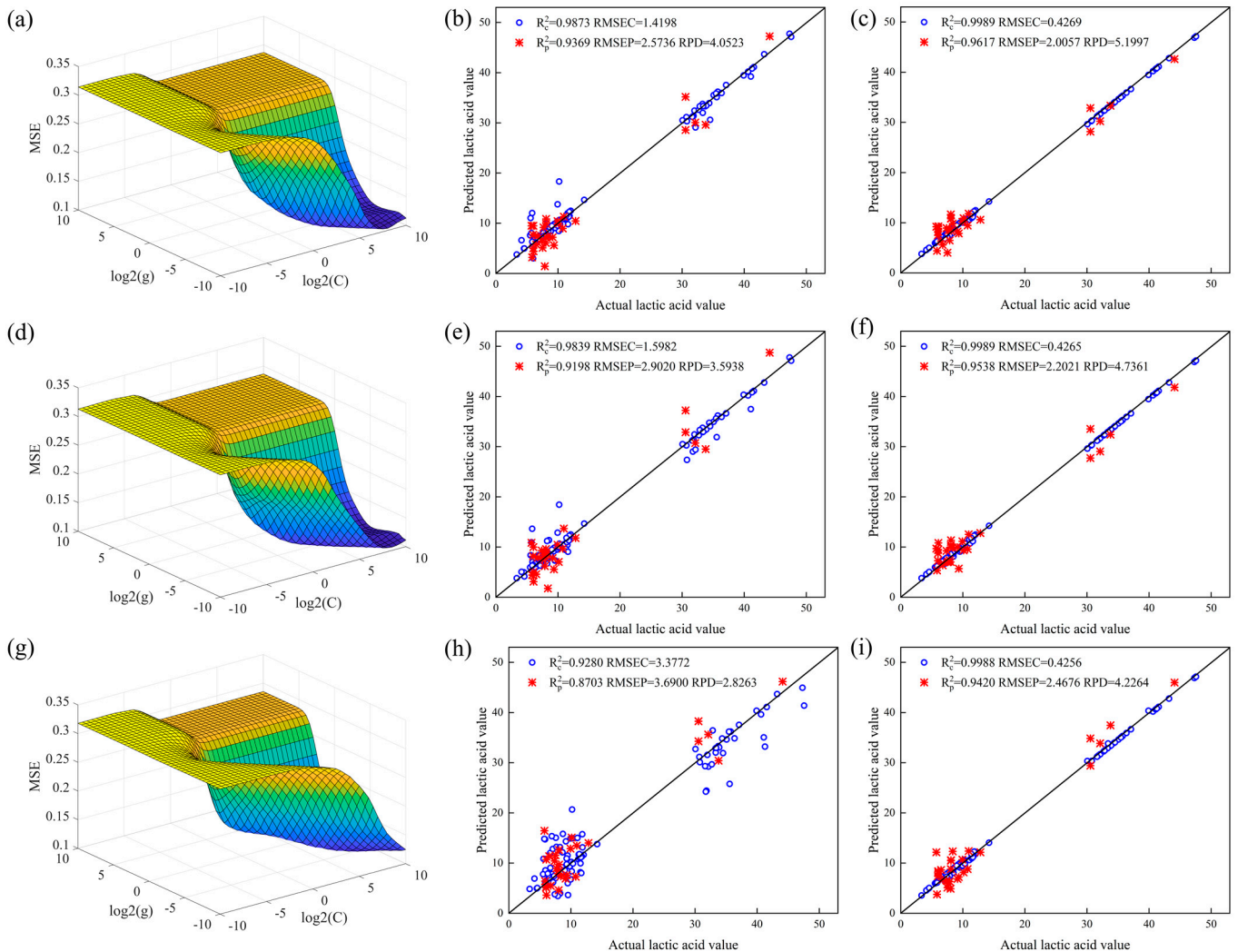


Figure 8. Model optimization based on SVR: (a) CARS-GS-SVR model parameter optimization; (b) regression between measured and predicted values of the CARS-GS-SVR model; (c) regression between measured and predicted values of the CARS-CPO-SVR model; (d) IRIV-GS-SVR model parameter optimization; (e) IRIV-GS-SVR model regression between measured and predicted values; (f) regression between measured and predicted values for the IRIV-CPO-SVR model; (g) VCPA-GS-SVR model parameter optimization; (h) regression between measured and predicted values for the VCPA-GS-SVR model; (i) regression between measured and predicted values for the VCPA-CPO-SVR model.

According to the above idea, the combination of the characteristic wavelengths of the three dyes extracted by the three variable screening methods of CARS, IRIV and VCPA was utilized as the model input to construct the CPO-SVR model. The regression between the predicted and measured values of the CPO-SVR model for the three feature extraction algorithms is shown in Figure 8c,f,i. Compared to the GS-SVR model, the CPO-SVR model showed higher prediction accuracy under all feature extraction algorithms.

Specifically, within the contexts of the CARS and IRIV algorithms, CPO optimization markedly enhanced the predictive capabilities of the models. When the value of c was 17.5906 and the value of g was 0.3574, the R_p^2 value of the CARS-CPO-SVR model was significantly improved to 0.9617, the value of $RMSEP$ decreased to 2.0057, and the value of RPD improved to 5.1997. When the value of c was 17.8146 and the value of g was 0.4959, the R_p^2 value of the IRIV-CPO-SVR model was significantly improved to 0.9538, the value of $RMSEP$ was reduced to 2.2021, and the value of RPD was improved to 4.7361. When the value of c was 33.2347 and the value of g was 1.8089, the R_p^2 value of the VCPA-CPO-SVR model was 0.9420 and the value of $RMSEP$ was 2.4676, which shows some enhancement but is still not as good as the CARS and IRIV algorithms.

3.7. Model Comparison

To identify a superior modeling approach for the rapid and precise prediction of lactate values, this study compared the performance of eight different models, with the results detailed in Table 4. The results showed that the RPD values of the five models were all greater than three after the screening of characteristic variables, indicating that the five models have good predictive ability and can be used to quantitatively predict the lactic acid content of maize silage. Modeled using the same feature extraction algorithm, the $RMSEP$ value of the prediction set of the CPO-SVR model was less than that of the GS-SVR model, while the R_p^2 and RPD values were higher than that of the GS-SVR model. Therefore, the CPO optimization algorithm improved the prediction accuracy of the SVR model compared to the GS algorithm. This suggests that the CPO-SVR model is well suited for predicting changes in the lactic acid content of maize silage. In addition, we found that the computational time of the CPO algorithm was significantly shorter compared to the traditional GS algorithm when modeled with the same feature extraction algorithm. This performance advantage is mainly attributed to the fact that the CPO algorithm mimics the porcupine's defense strategy, which effectively balances the exploration and exploitation process and accelerates the convergence through the periodic population reduction technique, thus reducing the overall computation time. The CPO optimization has the most significant effect on the SVR model enhancement of the CARS algorithm, while the IRIV algorithm shows stable prediction performance under both optimization conditions, which is consistent with the results of the feature wavelength screening. IRIV is a strategy that preserves both the strong and weak informational variables through iterative rounds. Although the R_p^2 value of the IRIV-CPO-SVR model was similar to that of the CARS-CPO-SVR model, the $RMSEP$ value was slightly higher, indicating that the CPO optimization was not as effective in enhancing the SVR model of the IRIV algorithm as it was for the CARS algorithm. This phenomenon may be the result of the gradual amplification of the noise information and discrepancy during the cycle iteration. In contrast, the SVR model prediction performance of the VCPA algorithm was relatively weak, especially under the GS optimization condition. Although CPO optimization improved the predictive performance of the SVR model of the VCPA algorithm, the overall performance was still weak. This may be due to the fact that the VCPA algorithm selected too few feature wavelengths, affecting the accuracy of the model predictions. Among the eight models, the CARS-CPO-SVR model had the largest R_p^2 and RPD values and the smallest $RMSEP$ value. This indicates that the CARS-CPO-SVR model has the best predictive ability among the eight models. Therefore, CARS-CPO-SVR was the best predictive model in this study for quickly and accurately estimating the lactic acid content of maize silage. The results of this study showed that the selection of appropriate feature extraction algorithms and optimization methods is important for improving the prediction accuracy of SVR models.

Table 4. Performance of different feature extraction algorithms for predictive modeling.

Models	Number of Input Features	Parameters	R_C^2	RMSEC	R_p^2	RMSEP	RPD
GS-SVR	1233	C = 181.0193, g = 0.0014	0.9967	0.7249	0.8554	3.8966	2.6765
CPO-SVR		C = 14.5275, g = 0.1379	0.9987	0.4407	0.8192	4.3576	2.3933
CARS-GS-SVR	196	C = 45.2548, g = 0.0078	0.9873	1.4198	0.9369	2.5736	4.0523
CARS-CPO-SVR		C = 17.5906, g = 0.3574	0.9989	0.4269	0.9617	2.0057	5.1997
IRIV-GS-SVR	173	C = 32, g = 0.0110	0.9839	1.5982	0.9198	2.9020	3.5938
IRIV-CPO-SVR		C = 17.8146, g = 0.4959	0.9989	0.4265	0.9538	2.2021	4.7361
VCPA-GS-SVR	32	C = 128, g = 0.0156	0.9280	3.3772	0.8703	3.6900	2.8263
VCPA-CPO-SVR		C = 33.2347, g = 1.8089	0.9988	0.4256	0.9420	2.4676	4.2264

4. Conclusions

This research validated the feasibility of employing a colorimetric sensor array combined with hyperspectral imaging technology to quantitatively assess the lactic acid content in maize silage after secondary fermentation. CSA were prepared using suitable color-sensitive dyes to collect volatile odor information from maize silage samples with different days of aerobic exposure. The raw spectral data were preprocessed using five distinct preprocessing algorithms, followed by the development of a partial least squares regression (PLSR) model. Based on the spectral information of the dyes processed using the optimal preprocessing algorithm, the CHIO algorithm was used to screen three color-sensitive dyes that are most sensitive to lactic acid in maize silage. Feature extraction was performed by three algorithms and SVR models were created using a combination of features from the three dyes as input. The results showed that during the secondary fermentation process, the lactic acid content initially decreased sharply due to the vigorous metabolism of aerobic microorganisms. As the exposure time extended, microbial activity reached an equilibrium, leading to the stabilization of lactic acid levels. For different color-sensitive dyes, choosing the appropriate preprocessing method can effectively reduce the noise information in the raw data and improve the model accuracy. The sensors composed of TPP#6, 8 and pH#5 screened based on the CHIO algorithm can effectively capture information on volatile organic compounds produced during the secondary fermentation of maize silage. The CARS algorithm has a better ability to search for important variables of the sensor and the CARS-CPO-SVR model is better able to characterize the quantitative analysis of the relationship between the dye spectral information and the lactic acid content. The CARS-CPO-SVR model obtained the best prediction accuracy compared to the CARS-GS-SVR model. These results provide a reference method for the application of a colorimetric sensor array combined with hyperspectral imaging in the quantitative analysis of feed lactic acid.

At present, since the collected olfactory information was obtained in a specific environment, as applied to field detection, systematic research on the issues of sensor stability and reproducibility are also required. Meanwhile, this study is preliminary and further research is needed to develop a portable device based on this method for on-site inspection. Of course, this is the direction of our team's future research efforts.

Author Contributions: Conceptualization, X.X., K.Z. and H.T.; methodology, X.X. and H.T.; software, X.X., K.Z. and Y.Y.; validation, H.T., K.Z. and Y.Y.; formal analysis, X.X., C.Z. and J.S.; investigation, Y.Y., Z.X. and C.Z.; resources, Z.X. and C.Z.; data curation, X.X.; writing—original draft preparation, X.X. and H.T.; writing—review and editing, X.X., H.T. and K.Z.; visualization, X.X.; supervision, H.T.; project administration, H.T.; funding acquisition, H.T. All authors have read and agreed to the published version of the manuscript.

Funding: This work was supported by the National Natural Science Foundation of China [32071893], the National Natural Science Foundation of China [52365035], the Natural Science Foundation of Inner Mongolia Autonomous Region [2024MS03019], the Innovation Calibration Program for College Students of Inner Mongolia Autonomous Region [202310129026], the Priority Agricultural

Engineering Projects [YLXKZX-NND-NYGCZD001] and the Inner Mongolia Autonomous Region “First-class Discipline Research Special Program” [YLXKZX-NND-046].

Institutional Review Board Statement: Not applicable.

Data Availability Statement: The data provided in this study are available upon request from the corresponding author. The data are not publicly available due to privacy needs.

Conflicts of Interest: The authors declare no conflicts of interest.

References

- Zhang, Y.; Li, D.; Wang, X.; Lin, Y.; Zhang, Q.; Chen, X.; Yang, F. Fermentation Quality and Aerobic Stability of Mulberry Silage Prepared with Lactic Acid Bacteria and Propionic Acid. *Anim. Sci. J.* **2019**, *90*, 513–522. [[CrossRef](#)] [[PubMed](#)]
- Li, Y.; Du, S.; Sun, L.; Cheng, Q.; Hao, J.; Lu, Q.; Ge, G.; Wang, Z.; Jia, Y. Effects of Lactic Acid Bacteria and Molasses Additives on Dynamic Fermentation Quality and Microbial Community of Native Grass Silage. *Front. Microbiol.* **2022**, *13*, 830121. [[CrossRef](#)] [[PubMed](#)]
- Okoye, C.O.; Wang, Y.; Gao, L.; Wu, Y.; Li, X.; Sun, J.; Jiang, J. The Performance of Lactic Acid Bacteria in Silage Production: A Review of Modern Biotechnology for Silage Improvement. *Microbiol. Res.* **2023**, *266*, 127212. [[CrossRef](#)] [[PubMed](#)]
- Wang, Y.-L.; Wang, W.-K.; Wu, Q.-C.; Zhang, F.; Li, W.-J.; Yang, Z.-M.; Bo, Y.-K.; Yang, H.-J. The Effect of Different Lactic Acid Bacteria Inoculants on Silage Quality, Phenolic Acid Profiles, Bacterial Community and In Vitro Rumen Fermentation Characteristic of Whole Corn Silage. *Fermentation* **2022**, *8*, 285. [[CrossRef](#)]
- Jiang, F.; Cheng, H.; Liu, D.; Wei, C.; An, W.; Wang, Y.; Sun, H.; Song, E. Treatment of Whole-Plant Corn Silage With Lactic Acid Bacteria and Organic Acid Enhances Quality by Elevating Acid Content, Reducing pH, and Inhibiting Undesirable Microorganisms. *Front. Microbiol.* **2020**, *11*, 593088. [[CrossRef](#)]
- Madrid, J.; Martínez-Teruel, A.; Hernández, F.; Megías, M.D. A Comparative Study on the Determination of Lactic Acid in Silage Juice by Colorimetric, High-Performance Liquid Chromatography and Enzymatic Methods. *J. Sci. Food Agric.* **1999**, *79*, 1722–1726. [[CrossRef](#)]
- Borreani, G.; Tabacco, E. Improving Corn Silage Quality in the Top Layer of Farm Bunker Silos through the Use of a Next-Generation Barrier Film with High Impermeability to Oxygen. *J. Dairy Sci.* **2014**, *97*, 2415–2426. [[CrossRef](#)]
- Ren, X.; Tian, H.; Zhao, K.; Li, D.; Xiao, Z.; Yu, Y.; Liu, F. Research on pH Value Detection Method during Maize Silage Secondary Fermentation Based on Computer Vision. *Agriculture* **2022**, *12*, 1623. [[CrossRef](#)]
- Serva, L.; Andrighetto, I.; Segato, S.; Marchesini, G.; Chinello, M.; Magrin, L. Assessment of Maize Silage Quality under Different Pre-Ensilage Conditions. *Data* **2023**, *8*, 117. [[CrossRef](#)]
- Pundir, C.S. Determination of Lactic Acid with Special Emphasis on Biosensing Methods: A Review. *Biosens. Bioelectron.* **2016**, *86*, 777–790. [[CrossRef](#)]
- Xiao-wei, H.; Xiao-bo, Z.; Ji-yong, S.; Zhi-hua, L.; Jie-wen, Z. Colorimetric Sensor Arrays Based on Chemo-Responsive Dyes for Food Odor Visualization. *Trends Food Sci. Technol.* **2018**, *81*, 90–107. [[CrossRef](#)]
- Suslick, B.A.; Feng, L.; Suslick, K.S. Discrimination of Complex Mixtures by a Colorimetric Sensor Array: Coffee Aromas. *Anal. Chem.* **2010**, *82*, 2067–2073. [[CrossRef](#)] [[PubMed](#)]
- Li, H.; Hu, Y.; Ma, S.; Haruna, S.A.; Chen, Q.; Zhu, W.; Xia, A. Porphyrin and pH Sensitive Dye-Based Colorimetric Sensor Array Coupled Chemometrics for Dynamic Monitoring of Tea Quality during Ultrasound-Assisted Fermentation. *Microchem. J.* **2024**, *197*, 109813. [[CrossRef](#)]
- Jiang, H.; Xu, W.; Chen, Q. Evaluating Aroma Quality of Black Tea by an Olfactory Visualization System: Selection of Feature Sensor Using Particle Swarm Optimization. *Food Res. Int.* **2019**, *126*, 108605. [[CrossRef](#)] [[PubMed](#)]
- Wang, J.; Jiang, H.; Chen, Q. High-Precision Recognition of Wheat Mildew Degree Based on Colorimetric Sensor Technique Combined with Multivariate Analysis. *Microchem. J.* **2021**, *168*, 106468. [[CrossRef](#)]
- Zhu, C.; Deng, J.; Jiang, H. Parameter Optimization of Support Vector Machine to Improve the Predictive Performance for Determination of Aflatoxin B1 in Peanuts by Olfactory Visualization Technique. *Molecules* **2022**, *27*, 6730. [[CrossRef](#)]
- Xu, W.; He, Y.; Li, J.; Deng, Y.; Xu, E.; Feng, J.; Ding, T.; Liu, D.; Wang, W. Non-Destructive Determination of Beef Freshness Based on Colorimetric Sensor Array and Multivariate Analysis. *Sens. Actuators B Chem.* **2022**, *369*, 132282. [[CrossRef](#)]
- Yang, M.; Zhai, X.; Huang, X.; Li, Z.; Shi, J.; Li, Q.; Zou, X.; Battino, M. Rapid Discrimination of Beer Based on Quantitative Aroma Determination Using Colorimetric Sensor Array. *Food Chem.* **2021**, *363*, 130297. [[CrossRef](#)]
- Liu, T.; Jiang, H.; Chen, Q. Qualitative Identification of Rice Actual Storage Period Using Olfactory Visualization Technique Combined with Chemometrics Analysis. *Microchem. J.* **2020**, *159*, 105339. [[CrossRef](#)]
- Jiang, H.; Liu, T.; He, P.; Chen, Q. Quantitative Analysis of Fatty Acid Value during Rice Storage Based on Olfactory Visualization Sensor Technology. *Sens. Actuators B Chem.* **2020**, *309*, 127816. [[CrossRef](#)]
- Liu, T.; Jiang, H.; Chen, Q. Input Features and Parameters Optimization Improved the Prediction Accuracy of Support Vector Regression Models Based on Colorimetric Sensor Data for Detection of Aflatoxin B1 in Corn. *Microchem. J.* **2022**, *178*, 107407. [[CrossRef](#)]

22. Jiang, H.; Deng, J.; Chen, Q. Olfactory Sensor Combined with Chemometrics Analysis to Determine Fatty Acid in Stored Wheat. *Food Control* **2023**, *153*, 109942. [[CrossRef](#)]
23. Zhao, M.; Liu, T.; Jiang, H. Quantitative Detection of Moisture Content of Corn by Olfactory Visualization Technology. *Microchem. J.* **2024**, *199*, 109937. [[CrossRef](#)]
24. Ouyang, Q.; Rong, Y.; Wu, J.; Wang, Z.; Lin, H.; Chen, Q. Application of Colorimetric Sensor Array Combined with Visible Near-Infrared Spectroscopy for the Matcha Classification. *Food Chem.* **2023**, *420*, 136078. [[CrossRef](#)]
25. Wang, S.; Chen, Q.; Han, Y.; Huang, S.; Wu, J.; Jiao, T.; Wei, J.; Chen, X.; Chen, Q. Non-Destructive Prediction of the Total Viable Count (TVC) in Fujian Oysters (*Crassostrea Angulata*) Based on the Colorimetric Sensor Array. *Microchem. J.* **2024**, *197*, 109911. [[CrossRef](#)]
26. An, T.; Li, Y.; Tian, X.; Fan, S.; Duan, D.; Zhao, C.; Huang, W.; Dong, C. Evaluation of Aroma Quality Using Multidimensional Olfactory Information during Black Tea Fermentation. *Sens. Actuators B Chem.* **2022**, *371*, 132518. [[CrossRef](#)]
27. Wang, Y.; Ren, Z.; Li, M.; Yuan, W.; Zhang, Z.; Ning, J. pH Indicator-Based Sensor Array in Combination with Hyperspectral Imaging for Intelligent Evaluation of Withering Degree during Processing of Black Tea. *Spectrochim. Acta Part A Mol. Biomol. Spectrosc.* **2022**, *271*, 120959. [[CrossRef](#)]
28. Li, L.; Li, M.; Cui, Q.; Liu, Y.; Chen, Y.; Wang, Y.; Zhang, Z.; Chen, Q.; Ning, J. Rapid Monitoring of Black Tea Fermentation Quality Based on a Solution-Phase Sensor Array Combined with UV-Visible Spectroscopy. *Food Chem.* **2022**, *377*, 131974. [[CrossRef](#)]
29. DB15/T 1458-2018; Determination of pH Value, Organic Acid and Ammonium Nitrogen in Silage. Inner Mongolia Autonomous Region Bureau of Quality and Technical Supervision: Hohhot, China, 2018.
30. He, H.-J. Simultaneous Quantifying and Visualizing Moisture, Ash and Protein Distribution in Sweet Potato [*Ipomoea Batatas* (L.) Lam] by NIR Hyperspectral Imaging. *Food Chem.* **2023**, *18*, 100631. [[CrossRef](#)]
31. Al-Betar, M.A.; Alyasser, Z.A.A.; Awadallah, M.A.; Abu Doush, I. Coronavirus Herd Immunity Optimizer (CHIO). *Neural Comput. Appl.* **2021**, *33*, 5011–5042. [[CrossRef](#)]
32. Abdel-Basset, M.; Mohamed, R.; Abouhawwash, M. Crested Porcupine Optimizer: A New Nature-Inspired Metaheuristic. *Knowl. Based Syst.* **2024**, *284*, 111257. [[CrossRef](#)]
33. Li, J.; Chen, L. Comparative Analysis of Models for Robust and Accurate Evaluation of Soluble Solids Content in 'Pinggu' Peaches by Hyperspectral Imaging. *Comput. Electron. Agric.* **2017**, *142*, 524–535. [[CrossRef](#)]
34. Jin, G.; Wang, Y.; Li, L.; Shen, S.; Deng, W.-W.; Zhang, Z.; Ning, J. Intelligent Evaluation of Black Tea Fermentation Degree by FT-NIR and Computer Vision Based on Data Fusion Strategy. *LWT Food Sci. Technol.* **2020**, *125*, 109216. [[CrossRef](#)]
35. Yao, K.; Sun, J.; Zhang, L.; Zhou, X.; Tian, Y.; Tang, N.; Wu, X. Nondestructive Detection for Egg Freshness Based on Hyperspectral Imaging Technology Combined with Harris Hawks Optimization Support Vector Regression. *J. Food Saf.* **2021**, *41*, 12888. [[CrossRef](#)]
36. Wang, Y.; Li, L.; Liu, Y.; Cui, Q.; Ning, J.; Zhang, Z. Enhanced Quality Monitoring during Black Tea Processing by the Fusion of NIRS and Computer Vision. *J. Food Eng.* **2021**, *304*, 110599. [[CrossRef](#)]
37. Zhang, Y.; Wu, L. Classification of Fruits Using Computer Vision and a Multiclass Support Vector Machine. *Sensors* **2012**, *12*, 12489–12505. [[CrossRef](#)]
38. Yu, S.; Bu, H.; Hu, X.; Dong, W.; Zhang, L. Establishment and Accuracy Evaluation of Cotton Leaf Chlorophyll Content Prediction Model Combined with Hyperspectral Image and Feature Variable Selection. *Agronomy* **2023**, *13*, 2120. [[CrossRef](#)]

Disclaimer/Publisher's Note: The statements, opinions and data contained in all publications are solely those of the individual author(s) and contributor(s) and not of MDPI and/or the editor(s). MDPI and/or the editor(s) disclaim responsibility for any injury to people or property resulting from any ideas, methods, instructions or products referred to in the content.